Interplay of Ionization and Sputtering with the Electron Cloud

G. Rumolo and F. Zimmermann

Abstract

The electron cloud enhances the generation and accumulation of ions, which in turn might increase both electron density and electron decay time. We report analytical considerations and simulations of ion motion under the combined influence of beam, electron cloud, and various external magnetic fields. From these, we infer ion survival times, ion impact energies and the equilibrium ion density. All of these are shown to be small. Only in a dipole field whose ion cyclotron frequency is resonant with the bunch spacing (2.62 T for hydrogen ions in the LHC) some ions may acquire kinetic energies of several keV. We argue that additional contributions from ion reflection and sputtering are insignificant.

1 Introduction

Ionization of the residual gas inside the beam pipe causes production of electrons as well as of positive ions, which then move under the action of the beam field forces and their own space charge. A known potential danger is the presence of electrons, from which a multipacting process may get started, which eventually leads to the build up of a quasi-stationary electron cloud. The gas ionization is especially important in proton machines like the SPS, for instance, where the photon energy of the synchrotron radiation is insuffcient to cause photoemission, which is the dominant source of primary electrons in the LHC at top energy.

An electron-cloud build up, presumably initiated by gas ionization and amplified via beam-induced multipacting, has been observed since 1999 at the CERN SPS [1, 2]. The electron-cloud build up in the beam pipe [3, 4, 5], as well as its consequences on the heat, on the beam diagnostics and on beam stability [6, 7] have been studied by computer simulations over the last few years.

Once the electron cloud is established, it will increase the rate of ion production in the beam pipe. The ionization cross section for a 100-eV electron is about 200 Mbarn, or 100 times larger than the ionization cross section for a high-energy beam proton [8]. Since at equilibrium the average numbers of beam particles and electrons are comparable, the cloud electrons may increase the ion production due to residual-gas ionization by two orders of magnitude.

The question whether the positive ions can be accumulated up to a density level sufficiently high to partially neutralize the electron space-charge field is the subject of this note.

First, in Section 2 we estimate the ion production rate for typical densities of the residual gas and the equilibrium electron cloud. Next, in Sections 3 and 4, we present rough analytical estimates of the ion survival times and impact energies. In Section 5, the dynamics of these ions under the influence of both the beam field and possible external fields, such as a dipole or a solenoid, is studied in more detail by means of computer simulations, in which the space-charge force of the electrons is taken into account. Ion elastic reflection and sputtering are addressed in Section 6. Finally, combining analytical and simulation results will eventually allow us in Section 7 to estimate the ion equilibrium density, before we draw some conclusions in Section 8.

2 Residual-Gas Ionization

The number density of residual gas molecules is given by

$$\rho_{\text{ion}} \approx \frac{p}{k_B T} \tag{1}$$

where p is the pressure in N/m^2, k_B Boltzmann's constant, and T the temperature. At a pressure of 1 nTorr (or 1.3×10^{-7} N/m^2), the residual gas density is $\rho_{\text{ion}} \approx 3 \times 10^{13}$ m^{-3}, one or two orders of magnitude higher than the equilibrium density of the electron cloud.

For electron energies of about 100 eV, ionization cross sections σ_{ioniz} are of the order 200 Mbarn [9]. For an electron density $\rho_e \approx 10^{11} - 10^{12}$ m^{-3} and average electron velocity $< v_e > \approx 6 \times 10^6$ m/s, which corresponds to 100 eV, a neutral atom is ionized at a rate of

$$\frac{1}{\tau_{\text{ion}}} \approx \sigma_{\text{ioniz}} \ < v_e > \ \rho_e \approx 0.012 - 0.12 \text{ s}^{-1}. \tag{2}$$

The ionization time of about 100 s is comparable to the KEKB hysteresis delay time [10].

3   Ion Energies

We estimate the kinetic energy of ions lost to the wall as

$$E_{\text{ion}} \approx \frac{e^2 Q N_b}{2\pi\epsilon_0 L_{\text{sep}}} \ln\left(\frac{r_b}{\sigma_r}\right) \tag{3}$$

where Q is the charge of the ion in units of the electron charge e, N_b the bunch population, L_{sep} the spacing, r_b the beam pipe radius, and σ_r the approximate rms transverse beam size, taken to be roughly equal to the horizontal rms beam size. In Eq. (3), we have assumed that the ionization takes places in the vicinity of the beam, we have neglected the bunched structure of the beam, and we have also assumed that no other field is acting on the ions apart from the beam field.

Inserting typical parameters listed in Table 1, we find the energies

$$E_{\text{ion}} \approx Q \ 103 \text{ eV} \qquad \text{for SPS,} \tag{4}$$

$$E_{\text{ion}} \approx Q \ 173 \text{ eV} \qquad \text{for LHC,} \tag{5}$$

$$E_{\text{ion}} \approx Q \ 180 \text{ eV} \qquad \text{for KEKB.} \tag{6}$$

Table 1: Some parameters for SPS, LHC (at top energy) and KEKB

machine	SPS	LHC	KEKB
approx. chamber radius r_b	30 mm	22 mm	47 mm
bunch population N_b	$\sim 10^{11}$	1.05×10^{11}	3.3×10^{10}
bunch spacing L_{sep}	7.5 m	7.5 m	2.4 m
approx. rms beam size σ_r	2 mm	0.3 mm	0.5 mm

The above estimate of ion energies will be refined in the following, where we consider two different field configurations (free space or dipole) in greater detail. Further below, in Section 5, a more accurate tracking simulation of the ion motion will be discussed. In all cases, we will confirm that the energy gain is independent of the ion mass.

We now estimate the maximum energy gained by an ion which is accelerated by a train of bunches both in a field-free drift space and in a dipole region. We estimate the final energy of an ion that is launched at the position $(x_0, 0)$. The ion having atomic mass number A gets a velocity boost from the first bunch $\Delta v_x(x_0)$ where

$$\Delta v_x(x_0) = \frac{2 r_p N_b c}{A} \ F_G(x_0, \sigma_x, \sigma_y) \tag{7}$$

and F_G can be expressed by the complex error function [11] and is normalized so that $|F_G(x)| \rightarrow 1/|x|$ for $x/\sigma_{x,y} \rightarrow \infty$. After the first bunch passage the ion drifts in the interbunch gap. When it reaches the position $x_1 = x_0 + \Delta v_x(x_0) T_{\text{sp}}$ where $T_{\text{sp}} = L_{\text{sep}}/c$, the next bunch passes. After N bunches, the ion will have come to the position $x_{N+1} = x_N + \left[\sum_{n=0}^{N} \Delta v_x(x_n)\right] T_{\text{sp}}$, and this process will stop for $N = M$, where M is defined by $x_M \geq r_x$ and $x_{M-1} < r_x$ (r_x is the pipe radius in the x-direction). The ion energy at this moment amounts to

$$E_{\text{ion}}^{\text{eV}}(x_0) = \frac{1}{2} \frac{A m_0}{e} \left[\sum_{n=0}^{M} \Delta v_x(x_n)\right]^2 \ , \tag{8}$$

where m_0 the proton mass, and we have assumed that the ion is still non-relativistic. Figure 1 shows the ion energy at the moment of impact on the wall, so computed, for different initial horizontal positions, considering a hydrogen ion and LHC parameters.

If we zoom in the region closer to the beam and pipe axis (lower graph in Fig. 1), we observe that the limit $\lim_{x_0 \to 0} E_{\text{ion}}(x_0)$ is not clearly defined because the function $E_{\text{ion}}(x_0)$ has an oscillating behaviour in the proximity of the origin with an amplitude varying between 150 and 220 eV. If we consider Cu^+ ions instead, we see in the upper picture of Fig. 2 that the impact energies are not very much different from those reached by hydrogen ions (protons), though the behaviour in the region $x_0 \to 0$ is more regular as $E_{\text{ion}} \overset{\sim}{\to} 170$ eV with no large amplitude oscillations. The lower picture of Fig. 2 demonstrates that the impact energy does in fact not depend on the ion mass, possibly except for very low initial x-positions and low mass numbers.

In the presence of an external dipole field $\vec{B} = (0, B, 0)$, the ion does not simply drift between two kicks, but it performs a cyclotron oscillation in the x–z plane (it still drifts as before in the y-direction). It is clear that, if no special resonance condition between the cyclotron period and the bunch spacing is met and if the cyclotron period is not much longer than the interbunch time T_{sp}, the ion will gain or lose energy randomly in the x-direction, moving back and forth on circular trajectories with different cyclotron radii. But the ion will also be accelerated bunch after bunch in the y-direction, as computed above for a drift space. The energy that the ion gains until it gets lost to the wall will therefore resemble the profile in Fig. 1, where on the x-axis one has to replace the initial horizontal position with the vertical one. A significant difference can occur for ions generated very close to the horizontal plane. The worst situation is encountered when the bunch spacing is an integer multiple of the ion cyclotron period, and the ion starts from an initial position near the x–z plane ($y_0 \approx 0$). In this case, the ion cumulatively gains energy since it is always at the same x position when a bunch arrives, and it does not move in the y-direction. Such ion will progressively move on circular trajectories with increasing radius and it will be lost only when its cyclotron motion intersects with the beam pipe. For other initial conditions, the ion could not gain as much energy, because it would quickly be accelerated to larger y values, further away from the beam, where in addition the available horizontal space becomes narrower.

For this reason, we now study the motion of an ion generated close to the horizontal plane. We consider an ion with the starting position $\vec{r}_0 = (x_0, 0, 0)$, and velocity $\vec{v}_0 = (\Delta v_x(x_0), 0, 0)$ (we assume that the ion has already received the kick from the first bunch having gone by). During the first interbunch gap, the motion of this ion will lie on the circle

$$[x(t) - x_0]^2 + \left[z(t) - \frac{\Delta v_x(x_0)}{\omega_c}\right]^2 = \left(\frac{\Delta v_x(x_0)}{\omega_c}\right)^2 \quad ,$$

where $\omega_c = ZeB/(Am_0) = N 2\pi/T_{\text{sp}}$. Ignoring the effect of the finite bunch length, when the next bunch comes, the ion will be again in its initial position. Therefore, after the passage of n bunches and prior to the arrival of the $n + 1$-th, the ion will move on the circle

$$[x(t) - x_0]^2 + \left[z(t) - n\frac{\Delta v_x(x_0)}{\omega_c}\right]^2 = \left(n\frac{\Delta v_x(x_0)}{\omega_c}\right)^2. \tag{9}$$

This also shows that its center of gyration will have drifted in the z-direction, as foreseeable ($\vec{E} \times \vec{B}$ drift). The condition of loss is

$$x_0 + r_c = r_x \quad , \tag{10}$$

where $r_c = M\Delta v_x(x_0)/\omega_c = T_{\rm sp}M\Delta v_x(x_0)/(2\pi)$ denotes the cyclotron radius. From Eq. (10), we derive the final ion velocity as

$$M\Delta v_x(x_0) = \frac{2\pi}{T_{\rm sp}}(r_x - x_0) \ , \tag{11}$$

and also the maximum total velocity gain

$$\lim_{x_0 \to 0} M\Delta v_x(x_0) = \frac{2\pi r_x}{T_{\rm sp}} \ .$$

For the LHC parameters with $r_x = 2.2$ cm and $T_{\rm sp} = 25$ ns and considering hydrogen ions, this yields a maximum energy gain of

$$E_{\rm ion} \approx 160 \text{ keV} \ ,$$

which will turn out to be an upper limit later, when we discuss results of simulation studies. The energy gain for a dipole field as a function of the initial horizontal ion position is plotted in Fig. 3.

4   Ion Survival Times

Outside the beam volume and assuming cylindrical symmetry, the motion of an ion is approximately described by the equation

$$\ddot{r} \approx \frac{e^2 Q N_B}{2\pi\epsilon_0 L_{\rm sep}m_0 A}\frac{1}{r} \tag{12}$$

for an unbunched beam. From this we can compute the survival time Δt of an ion launched with zero initial velocity at radial position r_0 as

$$\Delta t = \int_{r_0}^{r_b} \frac{dr}{\sqrt{2C\ln(r/r_0)}} \tag{13}$$

with $C = e^2 Q N_B/(2\pi\epsilon_0 L_{\rm sep}m_0 A)$. As an example, Fig. 4 shows typical survival times as a function of radial starting position for the LHC, SPS and KEKB.

Using exactly the same procedure as we did in the previous section, we can calculate the expected survival times of the ions for a bunched beam, either considering only the effect of the beam field or the combined effect of the beam and a dipole field, for an ion launched in the plane $y = 0$ (for different initial conditions, the survival time profile strongly resembles that for free space, because of the uniform acceleration in the y-direction). We use Eqs. (7) and (11), in order to compute M as a function of the initial x-position, where M represents the integer at which the summation over velocity increments must be terminated because the ion has reached the wall. From Eq. (11), M can be written as

$$M = \frac{2\pi}{T_{\rm sp}\Delta v_x(x_0)}(r_x - x_0) \ ,$$

and $\Delta v_x(x_0)$ is given by Eq. (7). In Fig. 5 the number of bunch passages until the loss of a hydrogen ion is depicted for the case of free space (upper picture) and for an LHC dipole field (lower picture), considering only ions launched in the horizontal plane.

Figure 6 shows the number of bunch passages before the ion loss in field-free space as a function of the initial horizontal position for copper ions (upper picture), and as a function of the ion mass for five fixed initial x-positions (lower picture). As we can see, the time that the Cu^+ ions take before hitting the wall is much higher than that required by the lighter hydrogen ions. The survival times grow monotonically for heavier ions.
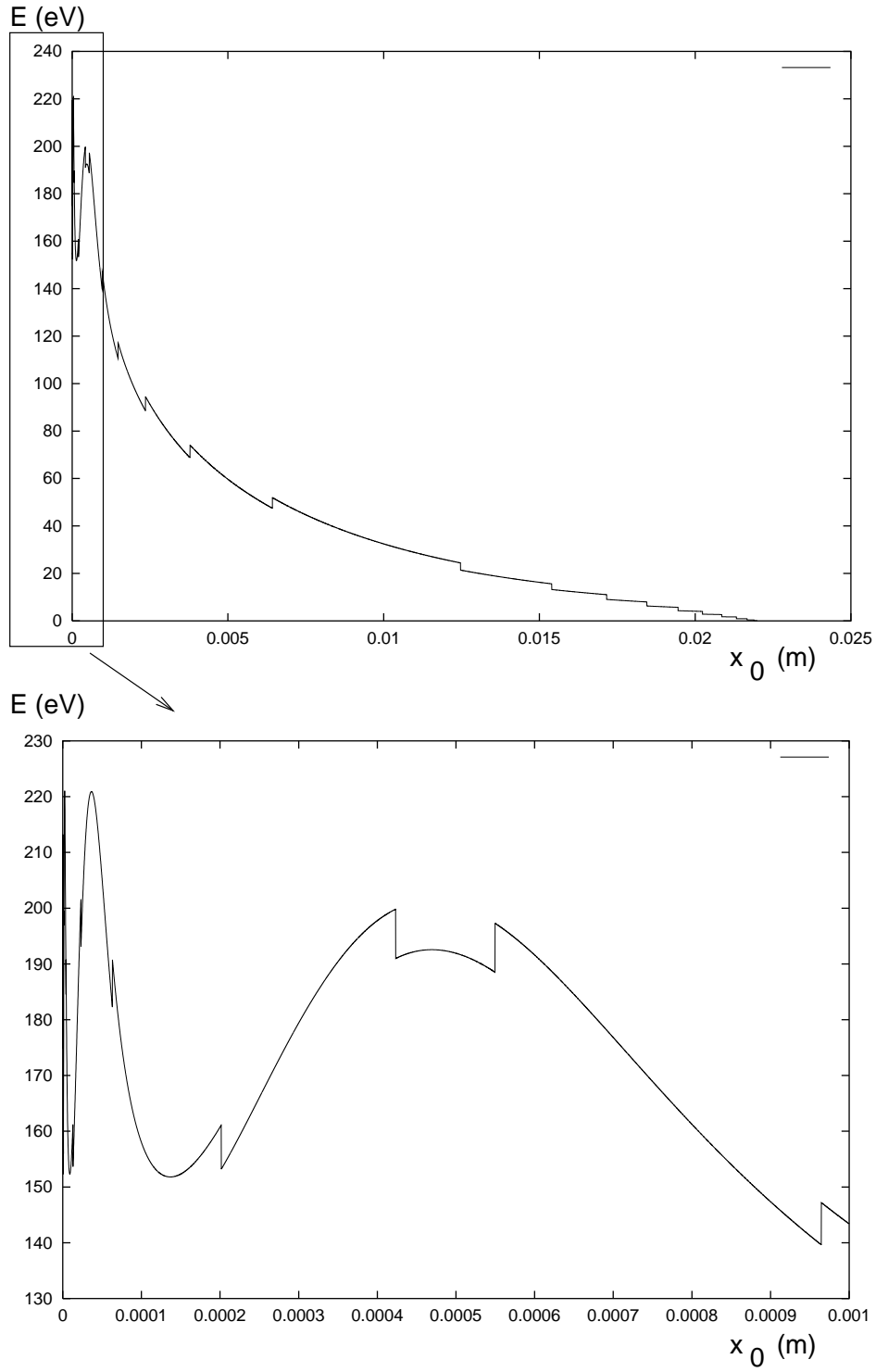
5

Figure 1: Proton energies at the moment of impact on the chamber wall in an LHC field-free region as a function of the initial horizontal position x_0 for $y_0 = 0$, according to Eq. (8).
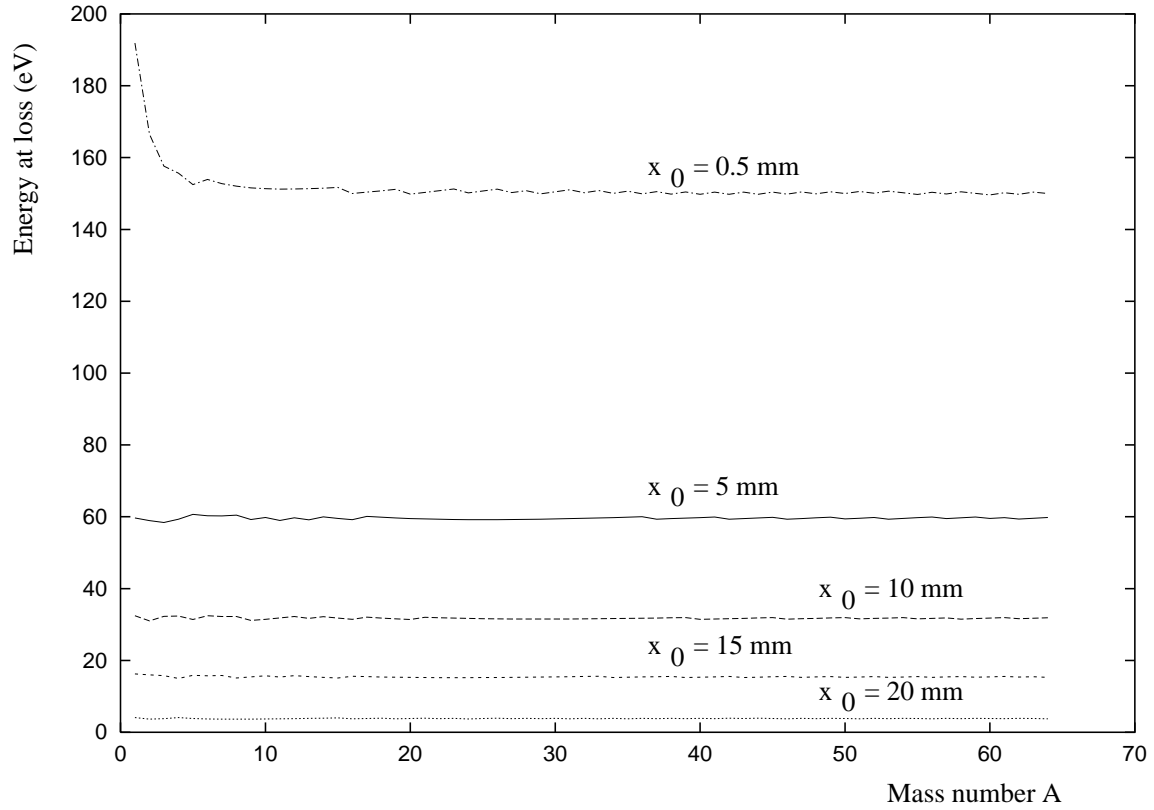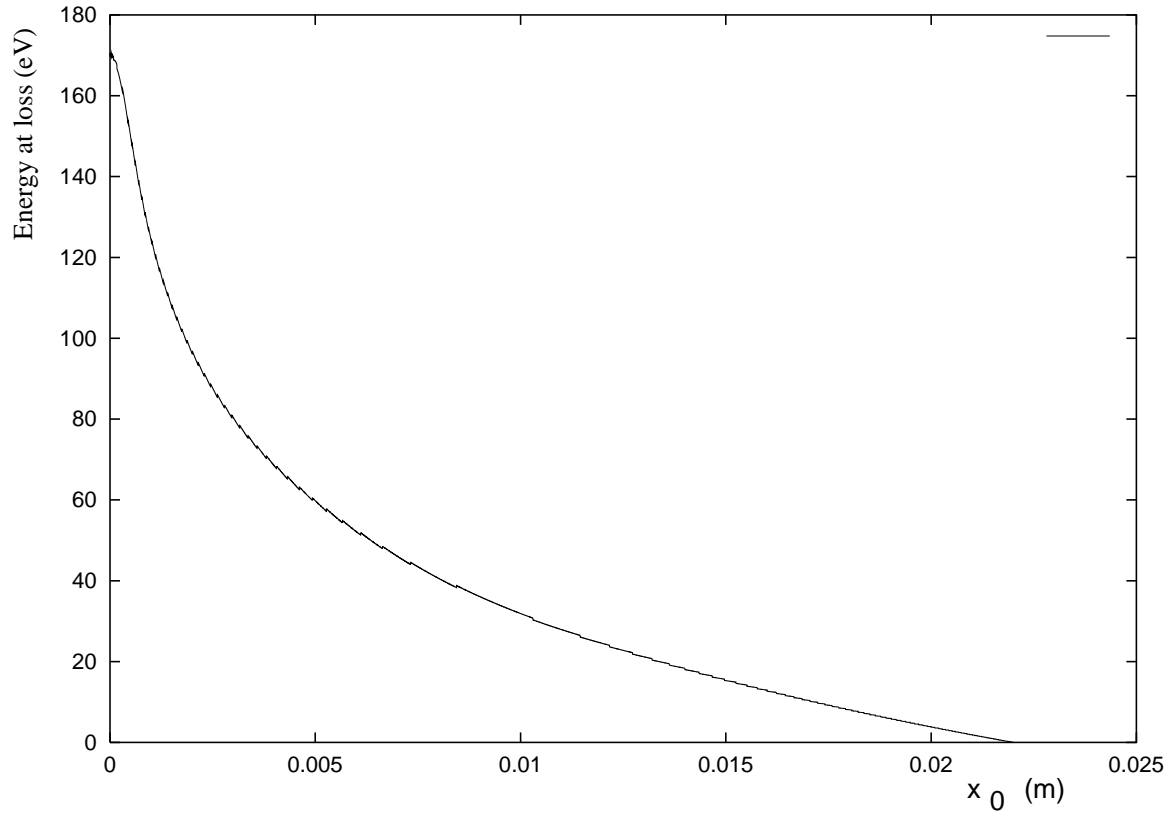
Figure 2: Impact energy in an LHC field-free region as a function of the initial x-position for copper ions (upper picture), and as a function of ion mass and for five different initial x-positions (lower picture).
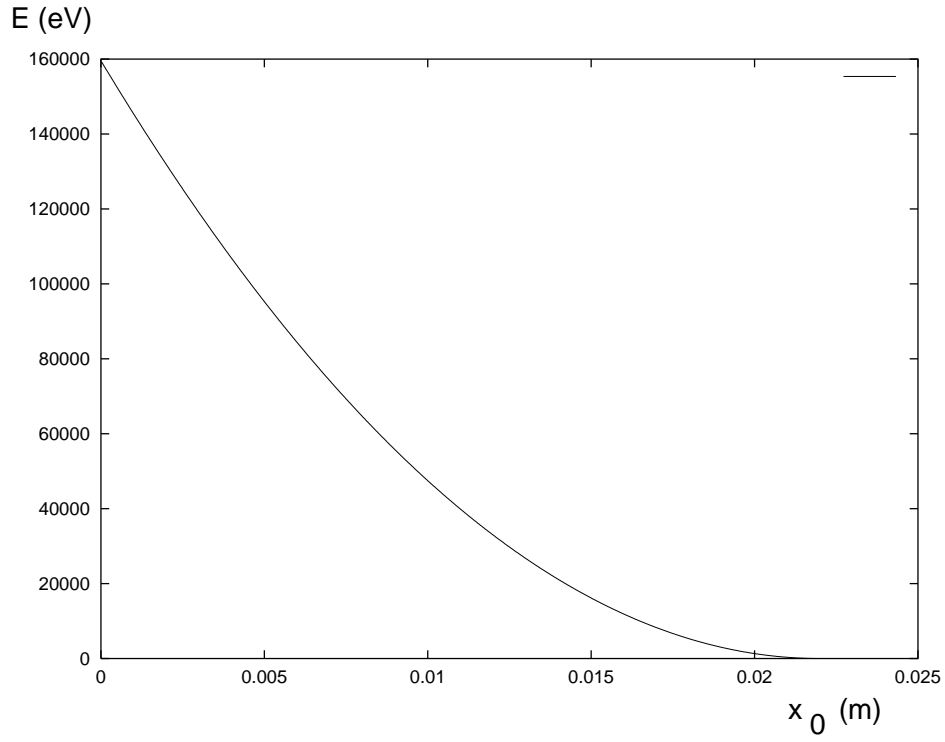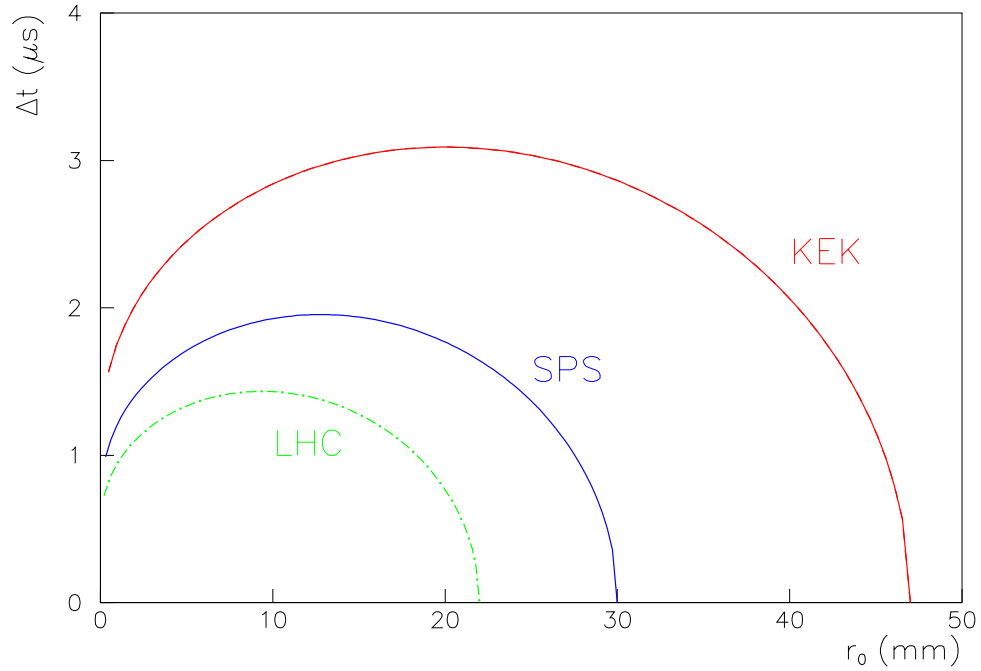
7

Figure 3: Ion energies at moment of impact on the chamber wall of an LHC dipole chamber as a function of the initial horizontal position x_0 for $y_0 = 0$, according to Eq. (11).

Figure 4: Ion survival times in s as a function of initial radial position in mm for $A = 28$ and $Q = 1$ (CO^+ or N_2^+) in the SPS, LHC and KEK B factory.
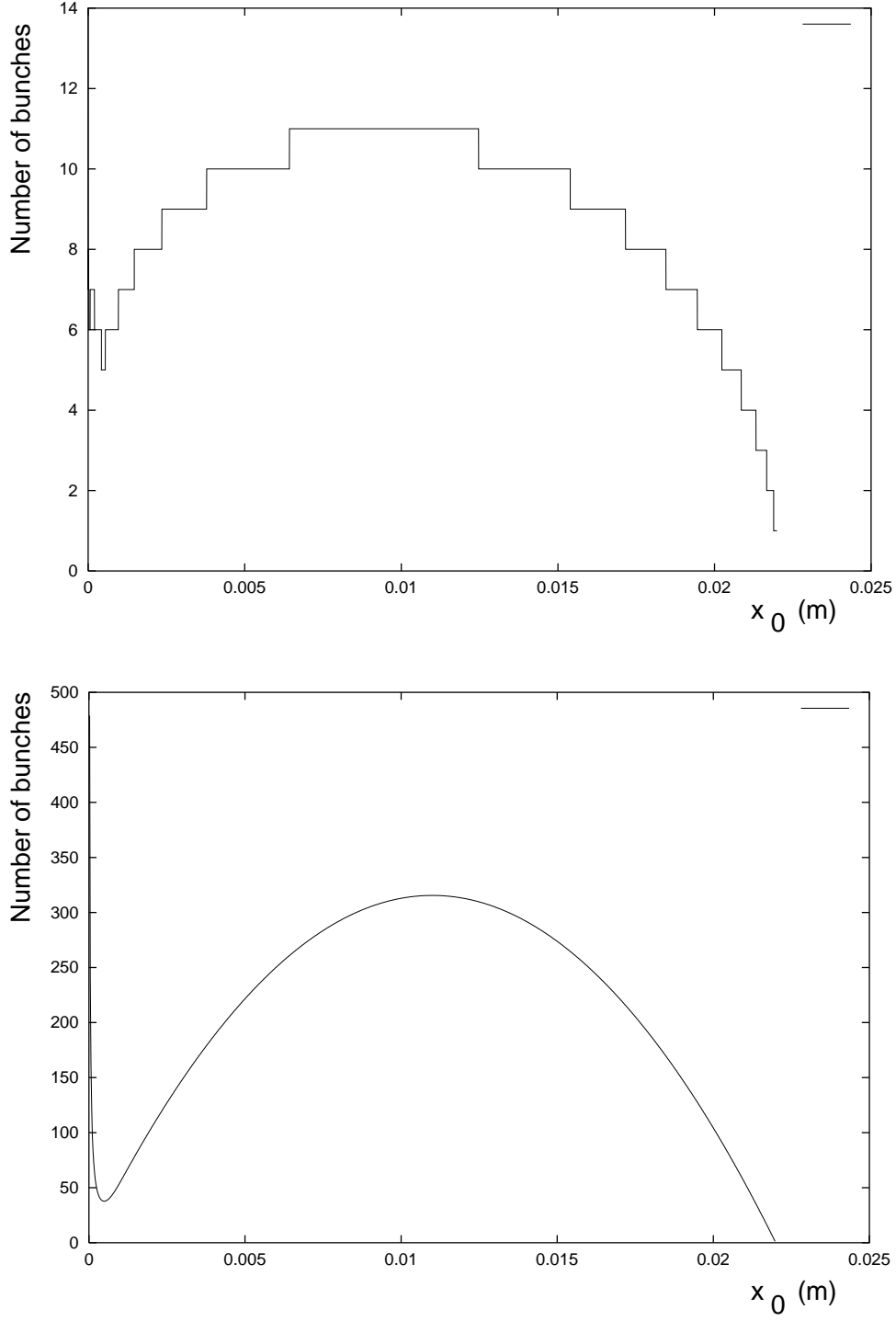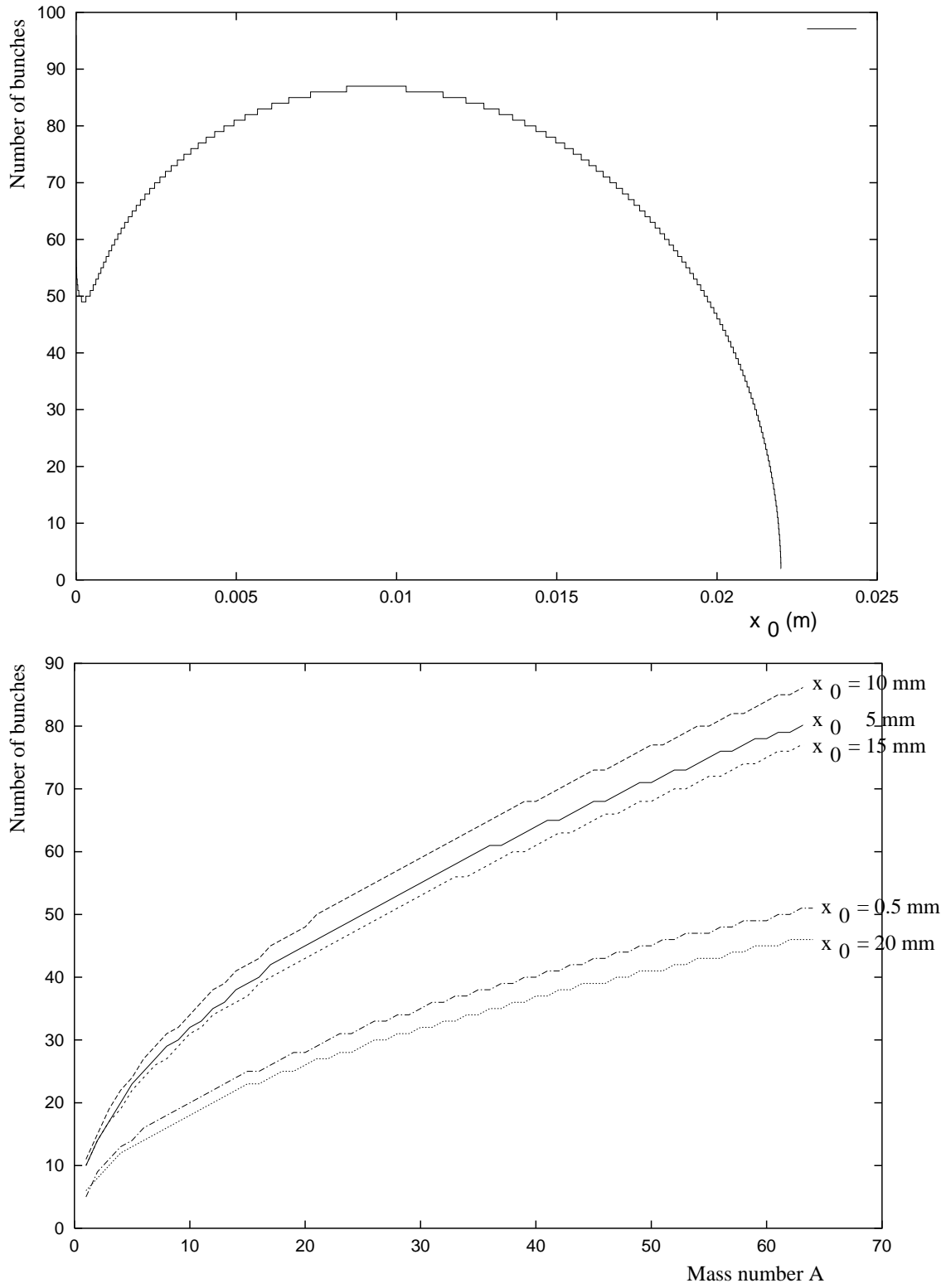
Figure 5: Ion survival times expressed in number of bunches as a function of initial horizontal position for H^+ in an LHC field-free region (upper curve) and in an LHC dipole on resonance (lower curve), for ions generated in the horizontal plane.

Figure 6: Ion survival time expressed in number of bunches as function of the initial horizontal position for Cu$^+$ in an LHC field-free region (upper picture), and as a function of the ion mass for the same five initial x-positions as considered in Fig. 2 (lower picture).

5 Ion Tracking

In order to estimate the number of positive ions inside the beam pipe, we have performed a series of ion tracking simulations, taking into account the effect of the beam field, the space charge force from the electron cloud, and optional external fields. This simulation has been carried out by modifying the existing electron tracking program [5]. Ions are produced at a bunch number that can be chosen in the input file and their motion is subsequently tracked under the forces of interest. The equations of motion for the ions in both dipole and solenoidal fields are solved by means of a 4-th order Runge-Kutta integrator. The motion of three different kinds of ions is followed. Their masses and charges are selected in the modified input file. An important parameter determined in the tracking is the survival time of the ions as a function of their initial position. From this, and using the production rate given in Section 2, we can estimate the equilibrium ion density. Another important parameter is the energy at the moment of impact. Depending on this energy the ions may be absorbed when they hit the wall, or, alternatively, they may be reflected, desorb gas molecules from the surface, or even cause sputtering of the chamber material [13, 14]. The probability of these processes will be estimated in the next section, based on the simulated ion impact energies.

In the simulations, we have always started from a uniform distribution of ions inside the beam pipe launched at a bunch number sufficiently high that the electron cloud had already fully built up beforehand. Comparing simulations in which the electron space-charge force on the ions was switched either on or off demonstrates that the main contribution to the motion of most ions is given by the beam field and that the electron-cloud space charge only has a small effect. This is understandable since the beam charge is confined to a small region in space and time, while the electrons are distributed over the entire chamber cross section, and since, in addition, on average the total number of electrons may be a factor 2–5 less than the number of beam particles.

Figures 7 and 8 depict the simulated survival times and impact energies for different kinds of ions in free space, as functions of their initial radial position. The numbers are in good agreement with our earlier estimates. Next, the density distributions for time and energy are displayed in Figs. 9 and 10. The figures illustrate that the survival times strongly depend on the ion mass. The heavier the ions, the longer they stay in the beam pipe. The maximum survival time for copper ions is about 2.2 μs.

On the other hand, as expected from Eq. (3), the energy of the lost ions does not much depend on the ion mass. In free space the energies are mostly of the order of a few eV, with a peak at 160-180 eV for those ions that start close to the beam at the center of the chamber. Figure 11 depicts trajectories in the x–y plane for 5 test particles, which are launched at a random point inside the pipe. In the absence of fields other than the nearly radial electric fields of the beam and the electron cloud, the ions are eventually lost to the wall after following straight trajectories.

Figure 12 displays the simulated survival times and impact energies for different kinds of ions, propagating without external magnetic fields, as a function of the initial radial position for the flat beam of KEKB. To exaggerate the effect, we here considered Cu^{2+} and CO^{2+} ions with a double charge, For single-charge ions, the loss times would be larger and the energies smaller by a factor 2.

In the presence of an LHC dipole field (vertical magnetic field of 8.39 T), the patterns of the survival times are less well defined. It appears that the survival times now extend toward higher values (upper picture in Fig. 13). The energy values are still low, with a maximum slightly above 160 eV (lower picture in Fig. 13). The trajectory and velocity of a single ion,
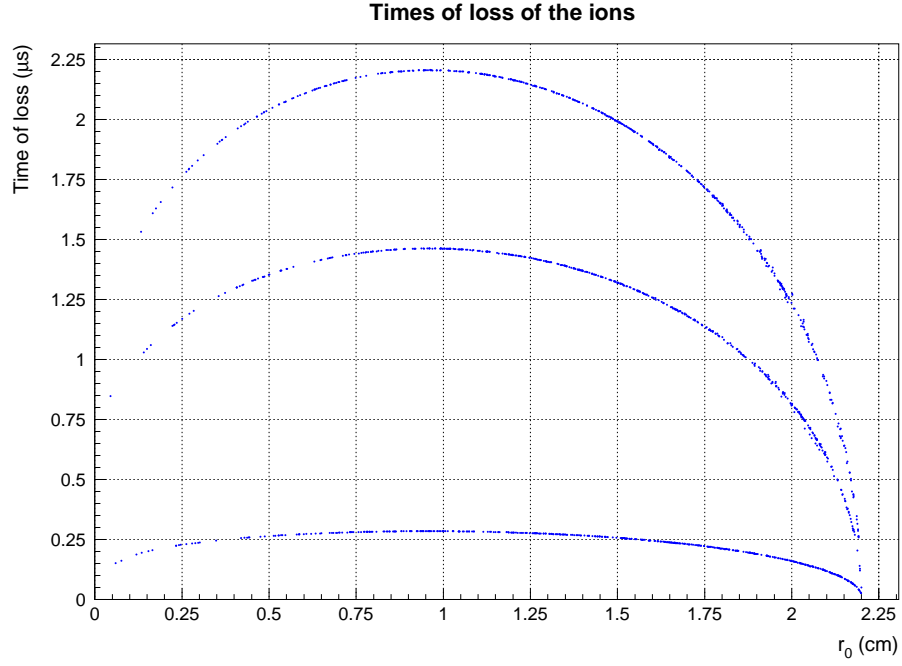
Times of loss of the ions

Figure 7: Survival times of ions as a function of the initial radial position, computed by launching ions in the electron-cloud simulation. The three curves represent the results for three different ion masses ($A = 1$, 28, and 64), all with $Q = 1$.
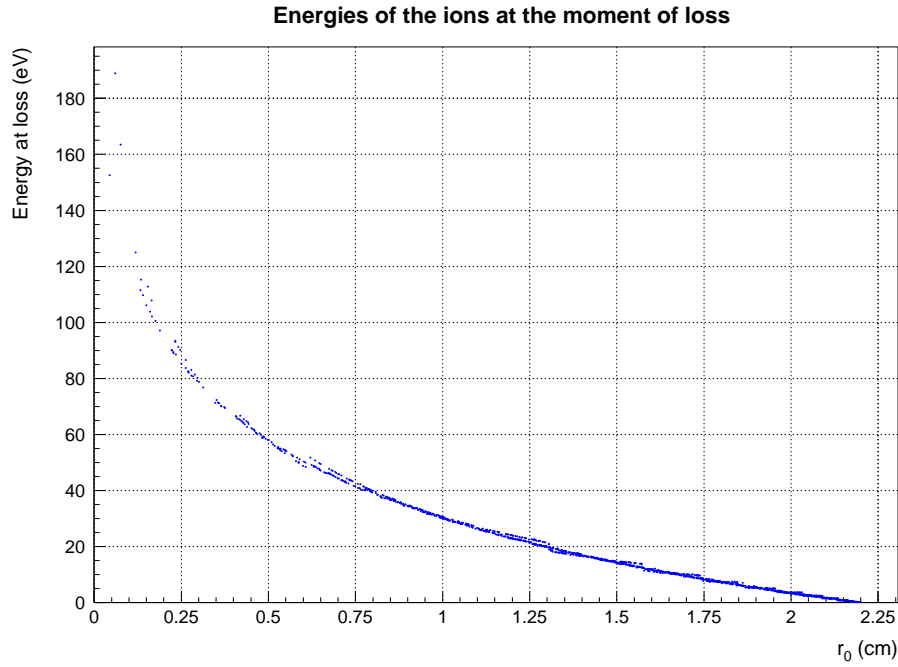
Energies of the ions at the moment of loss

Figure 8: Ion energies at moment of impact on the chamber wall as a function of the initial radial position for the LHC, computed by launching ions in the electron-cloud simulation. Results for three different ion masses are superimposed.
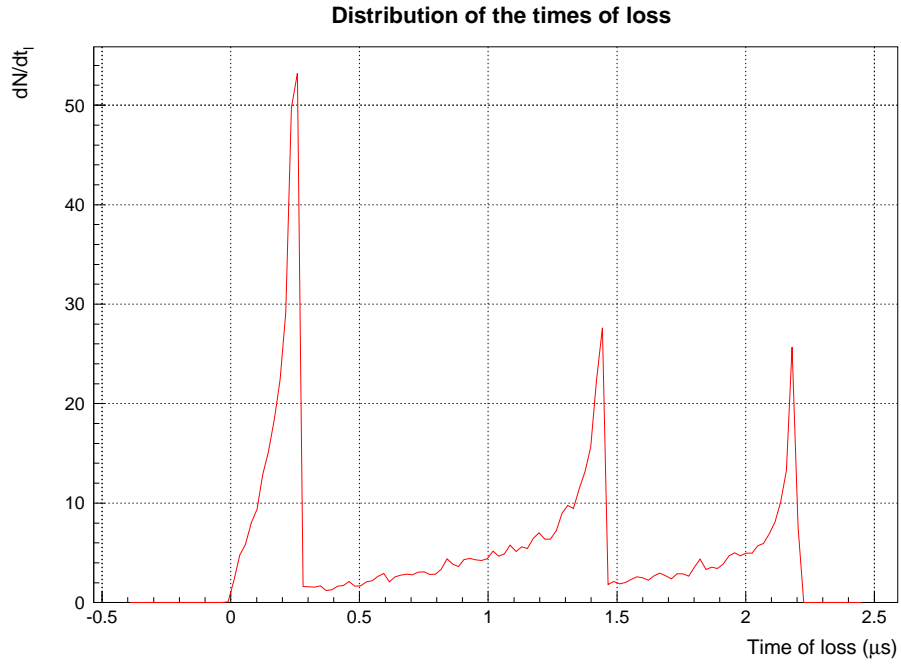
Figure 9: Distribution of survival times for three different ion species in the LHC. The peaks correspond to H^+, CO^+, and Cu^+, respectively.
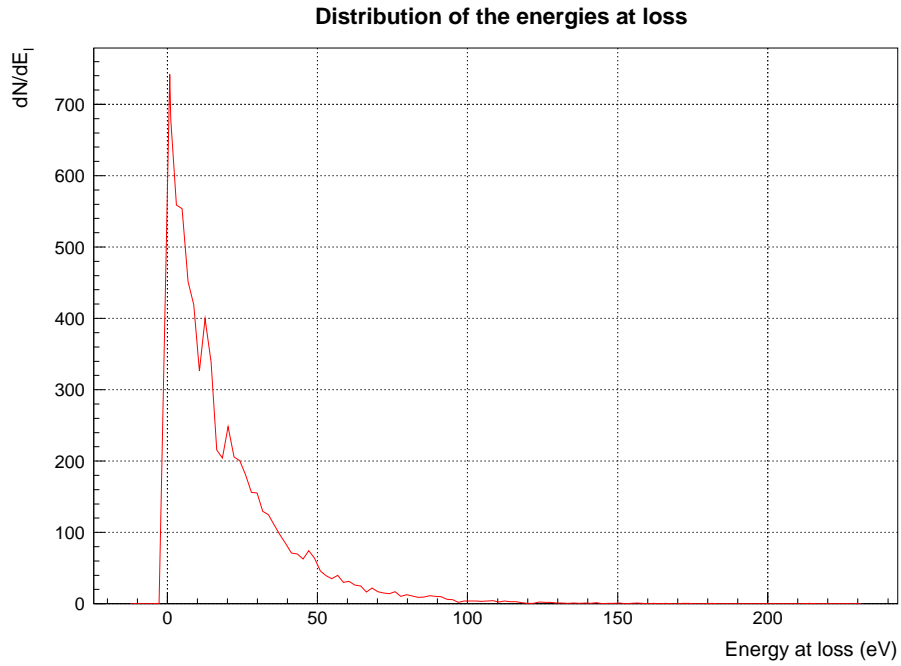

Figure 10: Distribution of impact energies in the LHC. Results for three different ion species are superimposed.
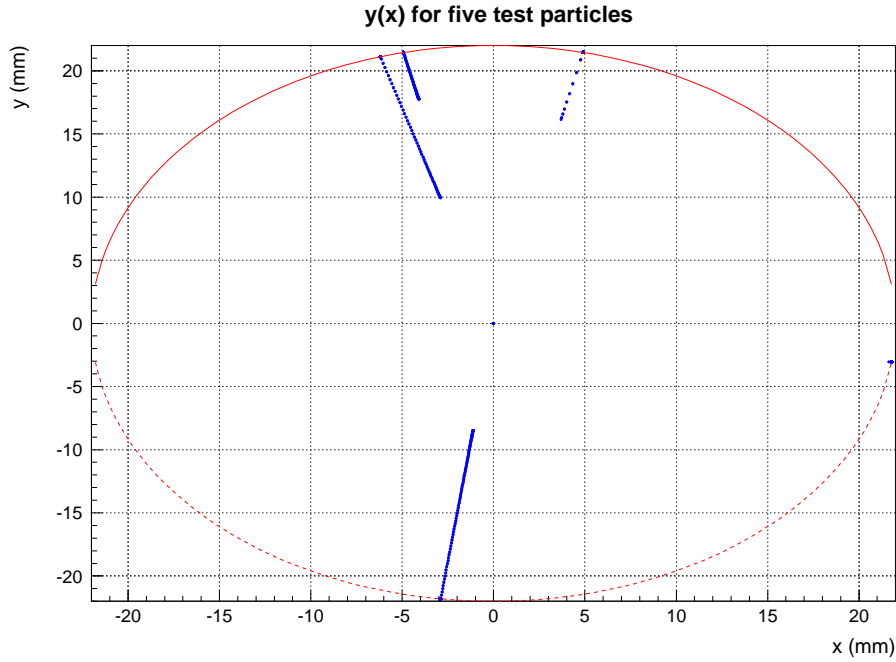
Figure 11: Trajectories of five test ions in the x–y plane, from the moment of their generation to their impact on the chamber wall.

plotted in Figs. 14 and 15, reveal the oscillatory motion in the x–z plane (with cyclotron radii that vary according to how much energy is gained or lost by the ion as a bunch passes by) and the accelerated motion in the y-direction.

It is particularly interesting to study the case of a magnetic dipole field for which the bunch spacing and the ion cyclotron period are in resonance. This happens, for instance, if we consider hydrogen ions (protons) in the LHC vacuum chamber under the effect of a 2.62 T field, for which

$$T_c = \frac{2\pi \mathrm{m}_p}{\mathrm{e}B} = 25 \text{ ns} \quad .$$

Computing the energies at the moment of loss for these hydrogen ions, we find that higher values are reached for small initial y coordinates (Fig. 16). The presumed resonance can be made more evident by plotting the single particle motion for one of these ions. Figures 17 and 18 reveal the growing amplitude of the x-z oscillation. The resonant energy gain is clearly visible in the $v_z(v_x)$ plane.

The theoretical limit decribed in Section 3 should be reached for ions which are created at very small initial y. We have performed a simulation in which we placed two of the ions close to the horizontal plane. The rest of the distribution was uniform and random. The results are depicted in Fig. 19. The energies gained by the two ions launched in the horizontal plane rise to 25-30 keV, but they fall short of the theoretical limit in Eq. (3). The discrepancy may be due to the decelerating effect of the electron cloud, not accounted for in our theoretical estimate. We also see that the ion does not remain exactly on resonance and thus does not gain the full energy boost on later cyclotron revolutions. In all cases, for which the vertical position is not exactly on the same plane as the beam, the ion quickly acquires momentum in the y-direction (the vertical electric field, is maximum for small x-values, as illustrated in Fig. 20).

The simulation for a weak solenoidal field, $e.g.$, for KEKB parameters, does not show large
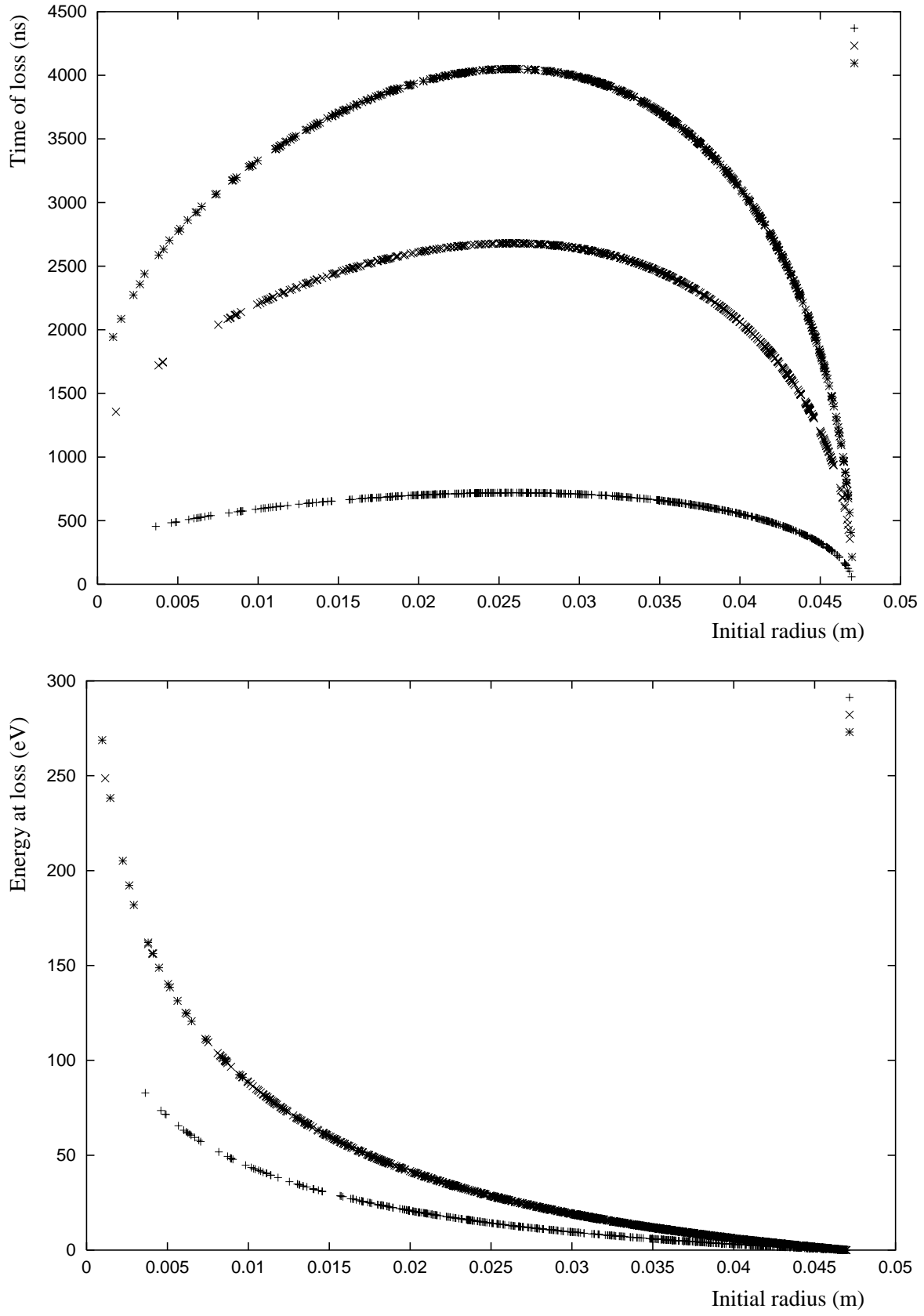
Figure 12: Survival times and energies as functions of the initial radial position for three different ion species (H^+, CO^{++}, and Cu^{++}) in a field-free region of KEKB.
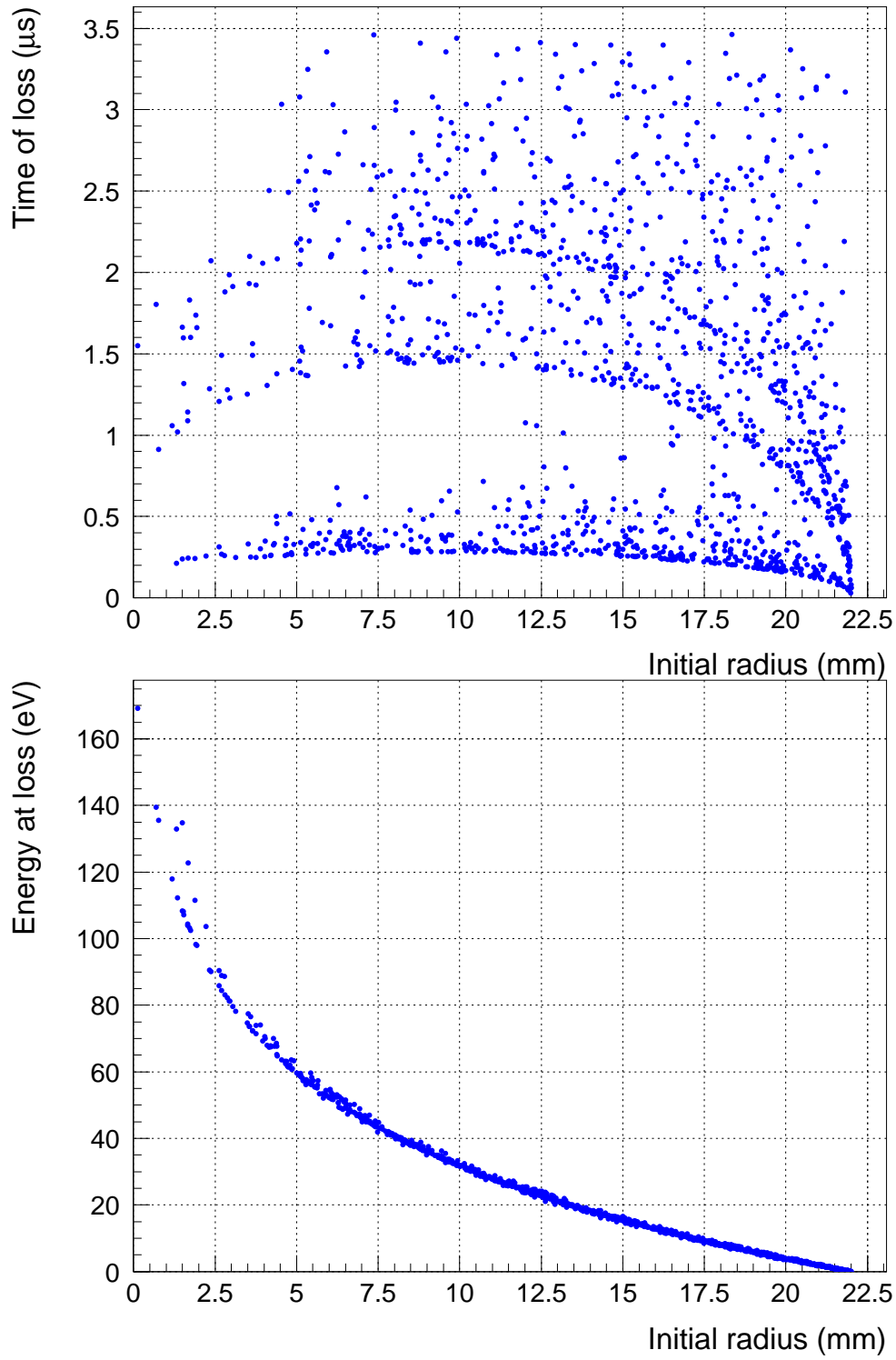
Figure 13: Survival times and energies as functions of the initial radial position for three different ion species (H^+, CO^+, and Cu^+) at the LHC in presence of a magnetic dipole field of 8.39 T.
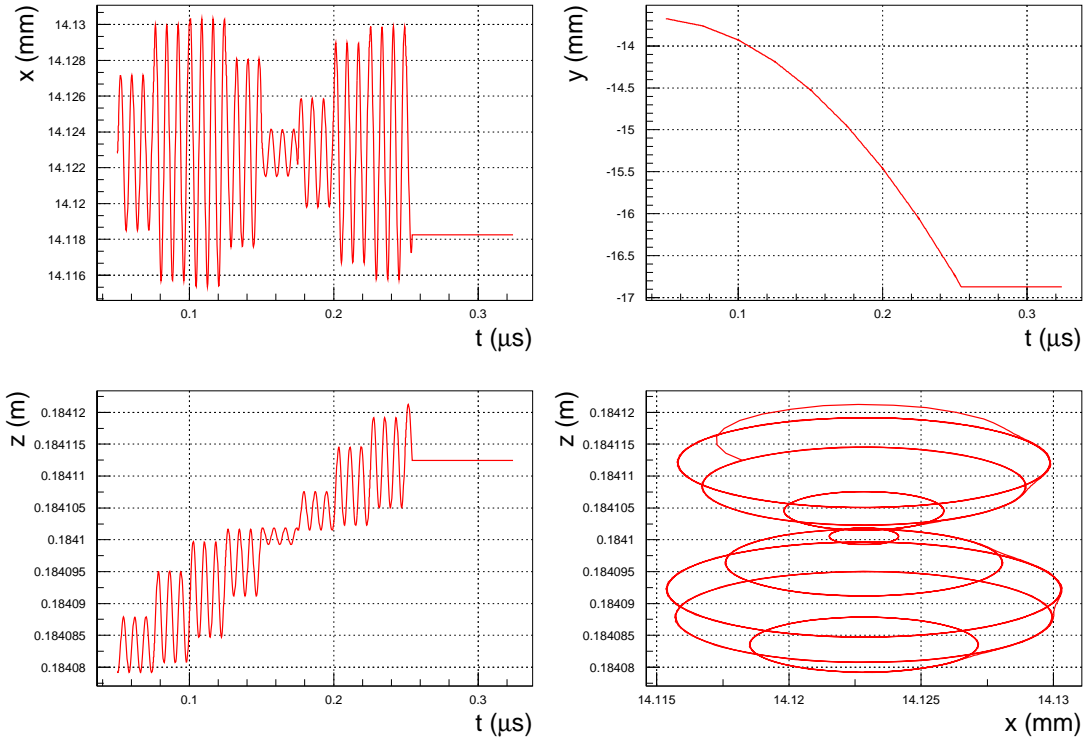
Figure 14: Coordinates $x(t)$, $y(t)$ and $z(t)$ for a hydrogen ion in an LHC dipole field of 8.39 T, under the influence of beam and electron space-charge forces. Bottom right picture shows the $z(x)$ trajectory.
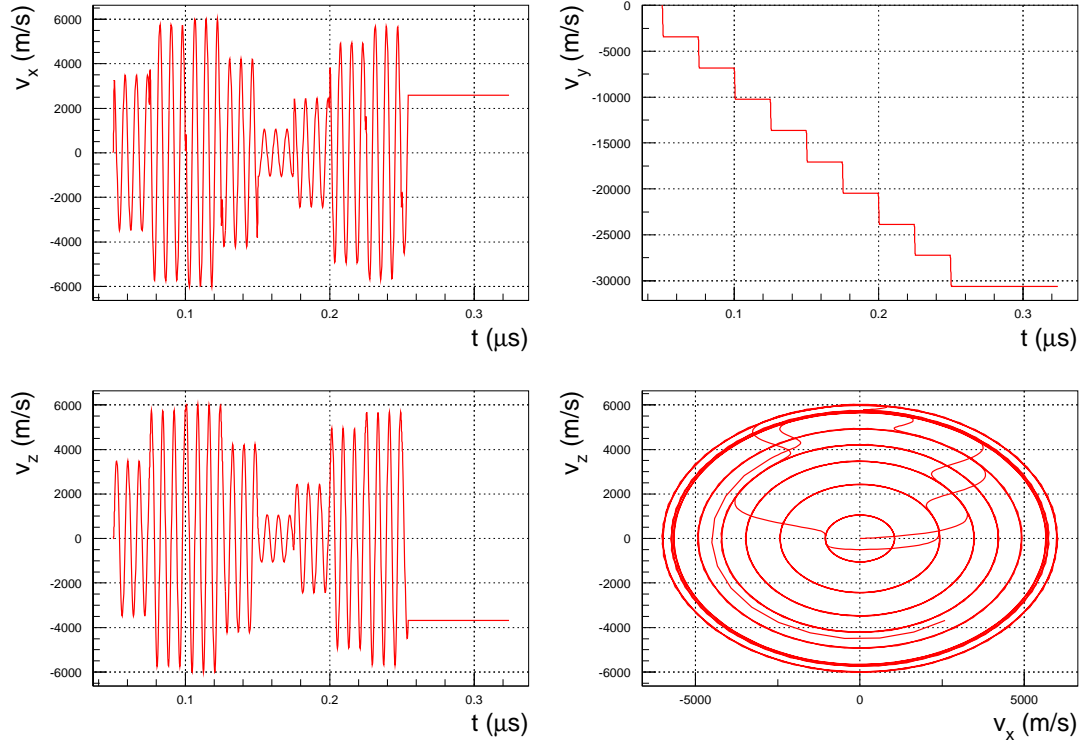
Figure 15: Velocities $v_x(t)$, $v_y(t)$ and $v_z(t)$ for a hydrogen ion in an LHC dipole field of 8.39 T, under the influence of beam and electron space-charge forces. Bottom right picture shows the $v_z(v_x)$ curve.
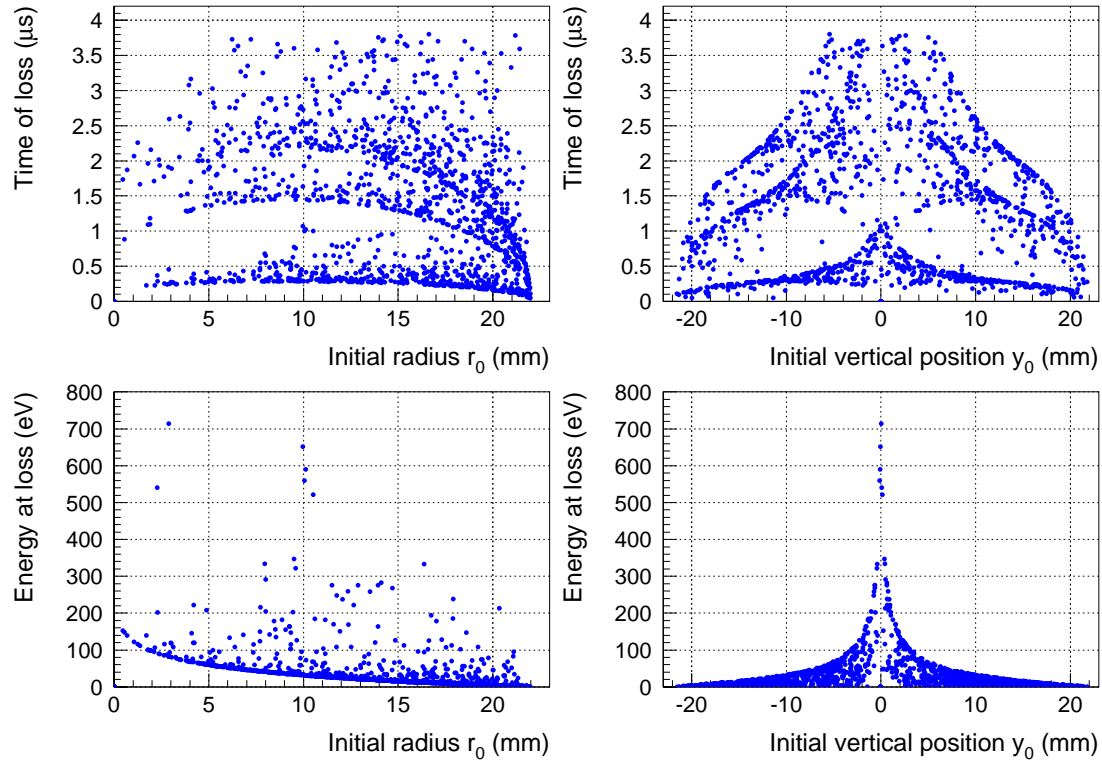
18

Figure 16: Survival times and energies as functions of the initial radial and vertical position for three different ion species (H^+, CO^+, and Cu^+) in the LHC in presence of a resonant magnetic dipole field.
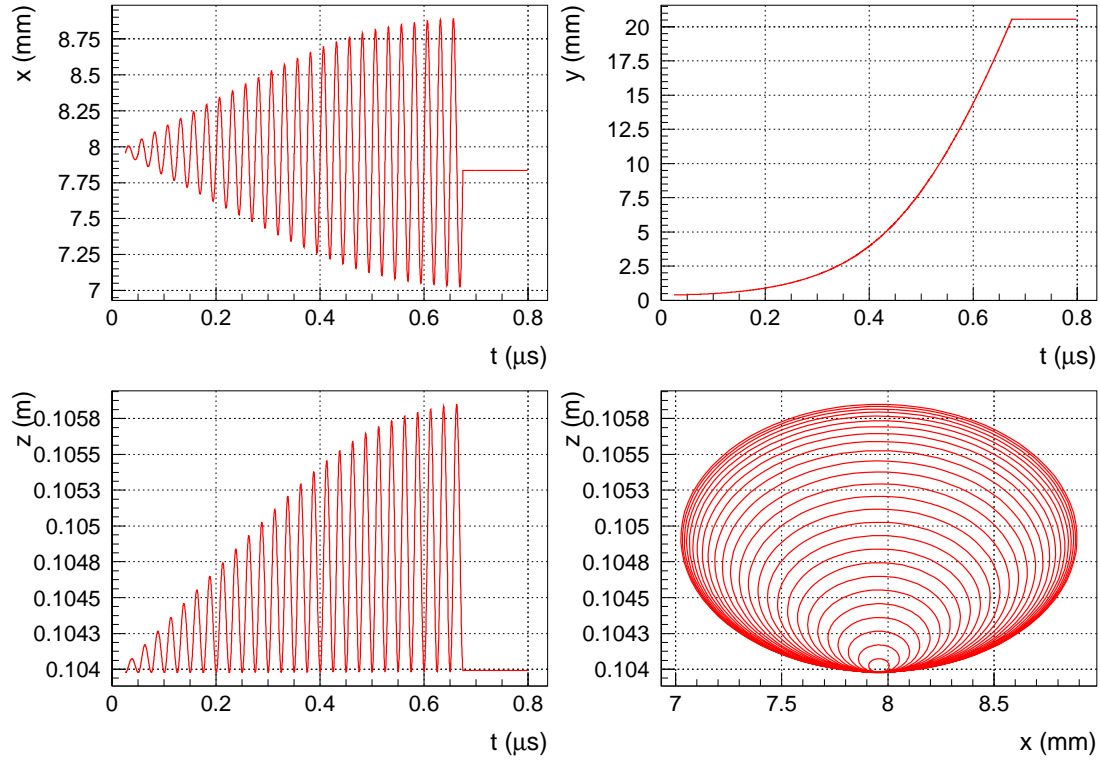
Figure 17: Coordinates $x(t)$, $y(t)$ and $z(t)$ for a hydrogen atom (proton) in a resonant LHC dipole field, under the influence of the beam and electron space-charge forces. The bottom right picture shows the $z(x)$ trajectory.
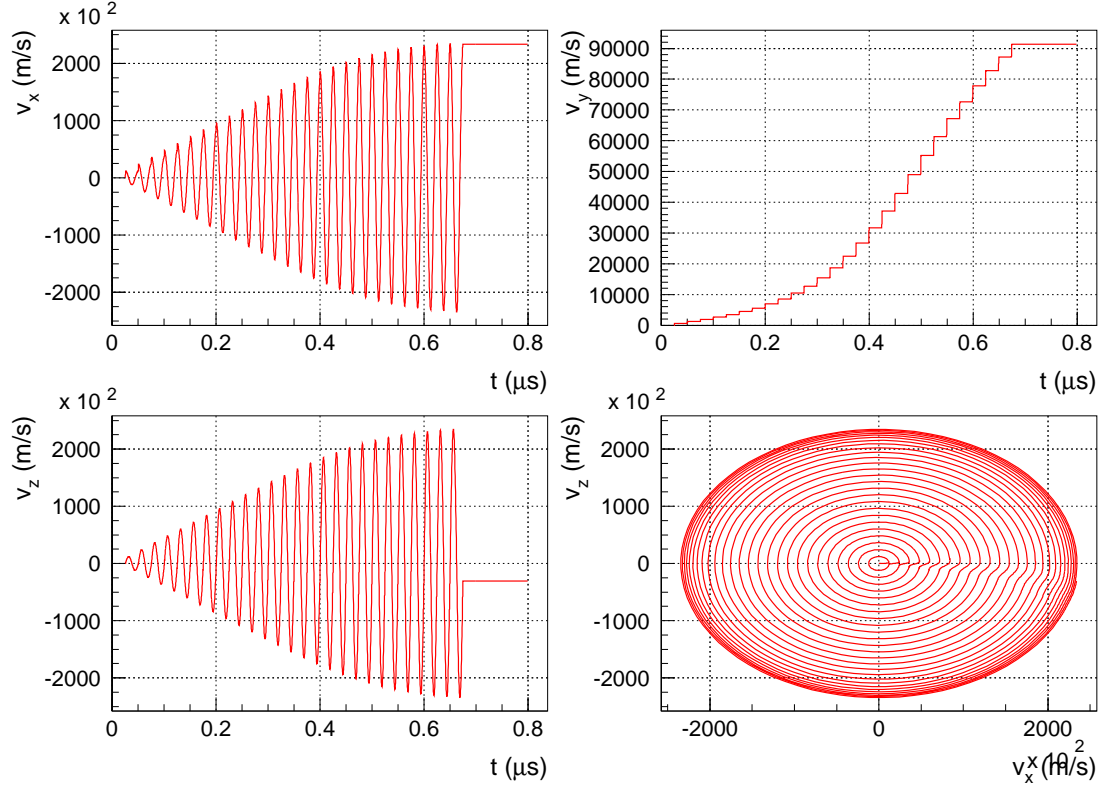
Figure 18: Velocities $v_x(t)$, $v_y(t)$ and $v_z(t)$ for a proton in a resonant LHC dipole field, under the effect of the beam and electron space-charge forces. The bottom right picture shows the $v_z(v_x)$ curve.
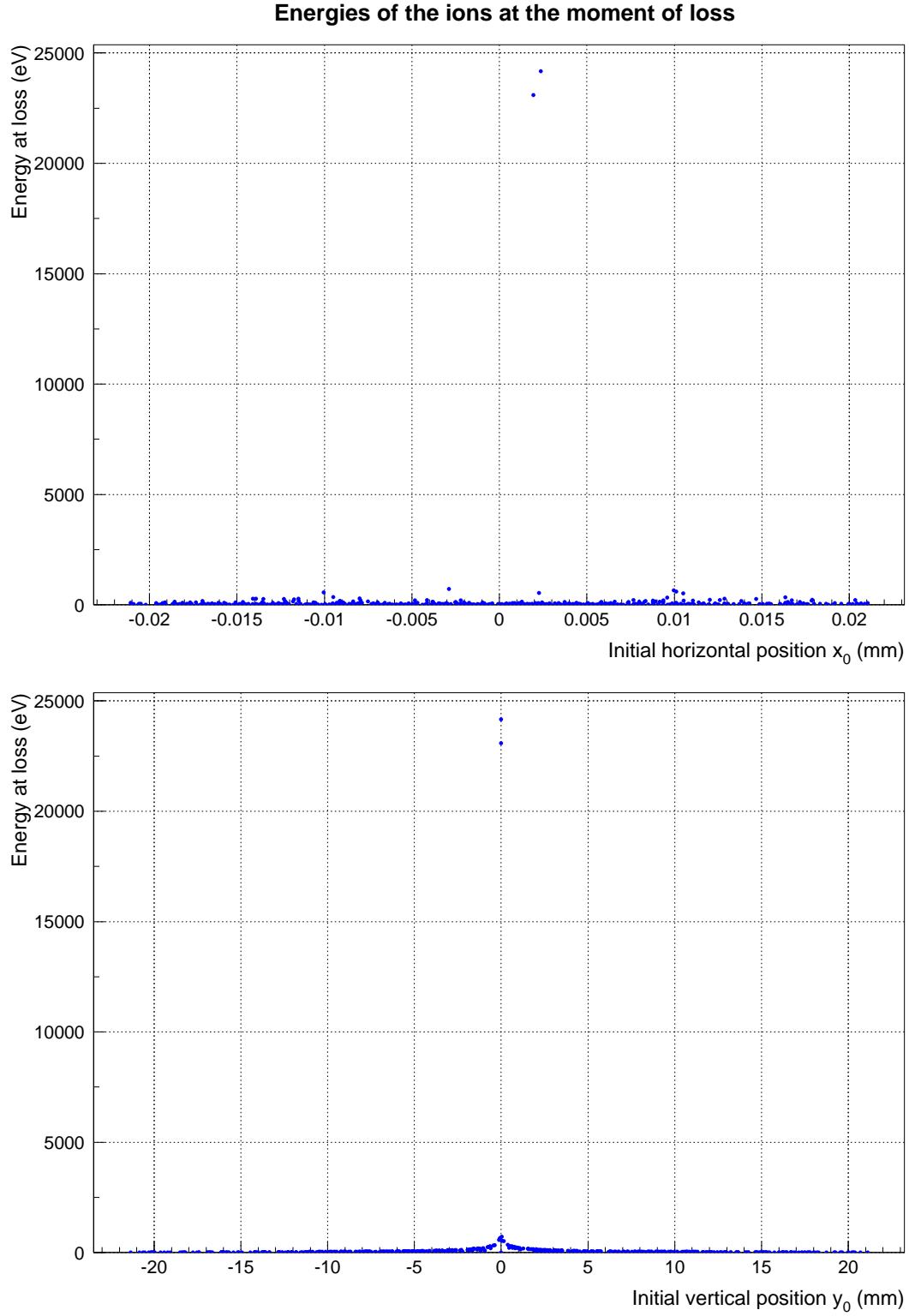
Energies of the ions at the moment of loss

Figure 19: Survival times and energies as functions of the initial horizontal and vertical position for three different ion species (H^+, CO^+, and Cu^+) in the LHC in presence of a resonant magnetic dipolar field. Two ions have been artificially generated very close to the horizontal plane.
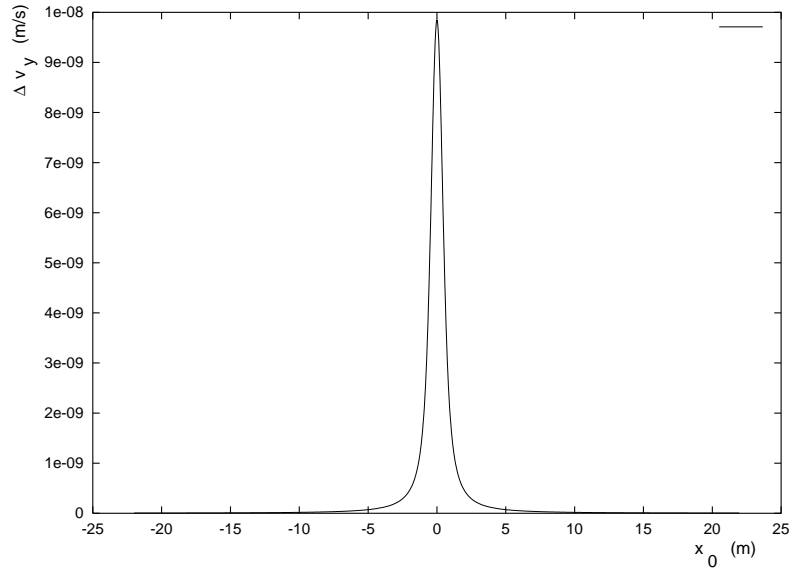
Figure 20: The net vertical kick Δv_y applied by a bunch to a hydrogen ion as a function of the ion initial position x_0, for fixed value of $y_0 = 1.87 \times 10^{-17}$ m.

differences with respect to the field-free case. A z-dependent periodic solenoidal field can be parametrized as [12]

$$B_r(r, z) = B_0 \frac{2}{\pi} ka \sum_{n=1}^{\infty} \sin nkh K_1(nka) I_1(nkr) \sin nkz$$

$$B_z(r, z) = B_0 \left[\frac{2h}{L} + \frac{2}{\pi} ka \sum_{n=1}^{\infty} \sin nkh K_1(nka) I_0(nkr) \cos nkz \right] \quad , \tag{14}$$

which is consistent with Maxwell's equations. In the equations above L is the period length, $2h$ the part of the period covered by windings, $k = 2\pi/L$, a the coil radius, and B_0 the field amplitude. A weak solenoid field is not expected to introduce a large perturbation of the ion motion with respect to the field-free case, because the ions are much heavier than the electrons. Survival times and energies at impact for hydrogen ions (protons) in KEKB with a solenoid field of 30 G are shown in Fig. 21. Not surprisingly, the effect of the weak solenoid field is indeed much smaller than the effect of a strong LHC dipole. Also for a solenoidal field, there could of course be a resonance phenomenon if the cyclotron period of the ions exactly equals the bunch spacing. However, for typical solenoid field strengths of 30–50 G, this situation does not occur. Therefore, this condition has not been investigated any further, in view of excessive computing time required for evaluating the expression of Eq. (14). Note that both series in Eq. (14) exhibit a poor convergence in the region $r \approx a$, which requires including a large number of terms in the two sums. In practical computation, the series should be extended through $n \approx L/|a - r|$ [12], which implies that we need at least 100 terms if we want to properly represent the field for particles up to a distance of 1 cm from the coil for a solenoid period of 1 m.
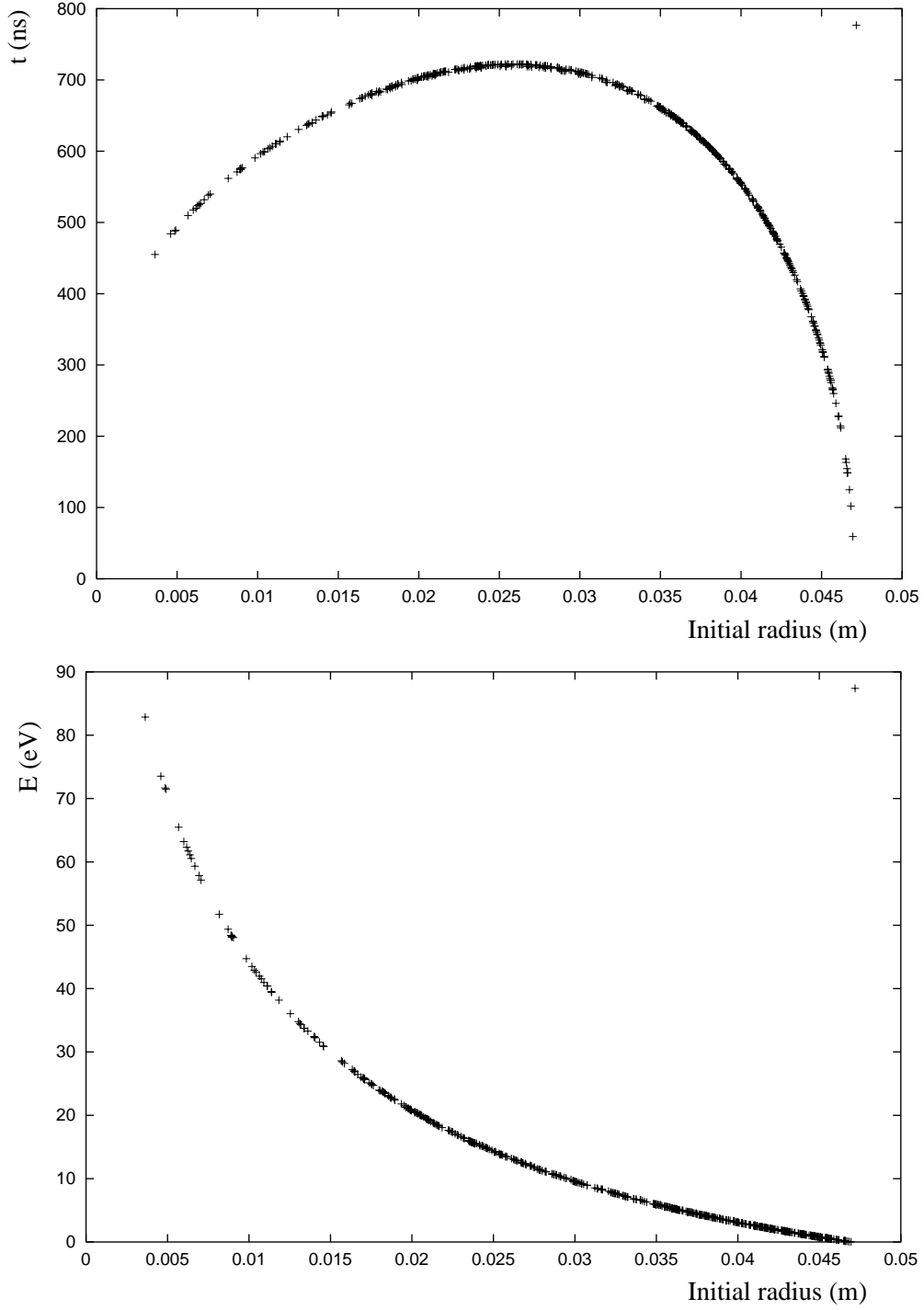
Figure 21: Survival times and energies as functions of the initial radius for H$^+$ in the KEKB LER in the presence of a magnetic solenoid field of 30 G that covers 80% of a 1 m long section. The coil radius a has been assumed to be equal to the beam pipe radius.

6 Reflection and Sputtering

In all simulations reported, we assumed that the ions are lost as they hit the inner wall of the beam pipe. From that moment on, they are simply "switched off". We now estimate the probability that these ions are really lost when they hit the beam pipe, instead of being back-scattered or giving rise to sputtering.

From references [13, 14] ("Reflection of light ions from solids" by W. Eckstein and H. Verbeek, pp. 12–28 of [13], and "Reflection" by W. Eckstein, pp. 17–31 of [14]), we infer that the reflection coefficients - defined as the ratio between the number of back-scattered particles and that of incident particles, and as the ratio between the total energy of the reflected particles and the total energy of the incident particles - increase as the energy of the projectile particles becomes smaller (which is only true down to a few eV; the reflection coefficients decrease again for even lower energies where the kinetic energy approaches the strength of the chemical binding forces on the surface). Reflection coefficients in the range 0.1-0.8 are found in the energy range 50–500 eV for protons impinging on copper (see graphs at pp. 16–17 of Ref. [13]). For incident ions of higher energy as well as for heavier projectiles, both reflection coefficients quickly drop to very low values. Coefficients in the order of few tenths may be interesting because they suggest that one or more ions out of ten are not lost to the wall upon impact but back-scattered, although with a lower energy.

Fortunately, most of the low-energy reflected particles are neutrals. The fraction of charged particles among the reflected particles is smaller than 15% for energies below 10 keV. In the range 50–500 eV, this percent even drops down to less than 4% (see graph at page 26 of Ref. [13]). All this taken into account, we estimate that the total net reflection coefficient for ions is not larger than 10^{-3}, and, thus, insignificant. Ion reflection can therefore be neglected when evaluating the total number of ions present inside the beam pipe.

A second phenomenon which could increase the number of ions and expand their lifetime is sputtering. Sputtering consists in the removal of target atoms by projectiles, and the sputtering yield is defined as the number of removed surface atoms per incident projectile ("Physical sputtering" by W. Eckstein, J. Bohdansky and J. Roth, pp. 51–63 in [14]).

We can compute the amount of sputtering expected for protons impinging on copper as well as for copper ions on copper by using an approximate analytical formula valid for normal incidence,

$$Y_{\mathrm{sput}}(E_0) = Q \frac{3.441\sqrt{E_0/E_{\mathrm{TF}}}\ln(E_0/E_{\mathrm{TF}} + 2.718)}{1 + 6.355\sqrt{E_0/E_{\mathrm{TF}}} + E_0/E_{\mathrm{TF}}(6.882\sqrt{E_0/E_{\mathrm{TF}}} - 1.708)} .$$

$$\cdot \left[1 - \left(\frac{E_{\mathrm{th}}}{E_0}\right)^{2/3}\right]\left(1 - \frac{E_{\mathrm{th}}}{E_0}\right)^2 \tag{15}$$

where E_0 is the energy of the incident particle, and parametrizations for Q, E_{TF} and E_{th} are given in Refs. [14, 15]. For Copper, $Q = 17$ atoms/ion, $E_{\mathrm{TF}} \approx 225$ keV, $E_{\mathrm{th}} \approx 36$ eV. Figure 22 shows that sputtering of copper from light ions is not expected to deliver much, since the sputtering yield always stays much lower than unity in the range of typical ion impact energies. Self-sputtering of copper ions could in principle be more dangerous, because its yield exceeds unity already for incident energies in the order of a few hundred eV. But as our ion tracking study has shown, not many ions are accelerated to even those moderate energies. Copper ions are far too heavy to fulfill the resonant condition between bunch spacing and cyclotron motion for LHC parameters. In a field-free region, they are never accelerated to more than 150 eV.

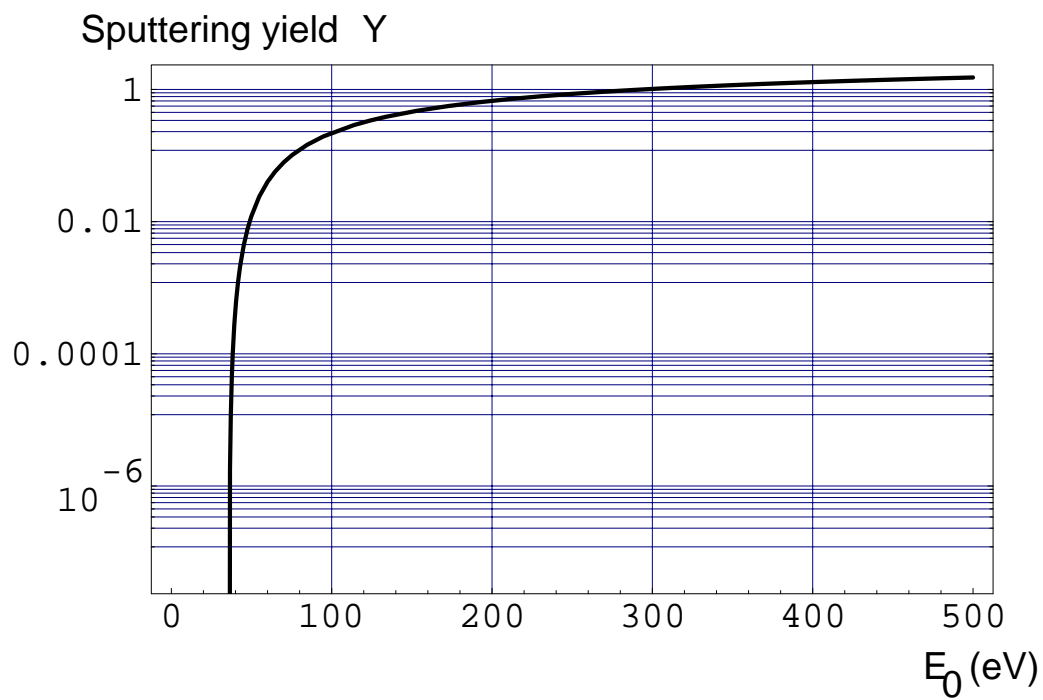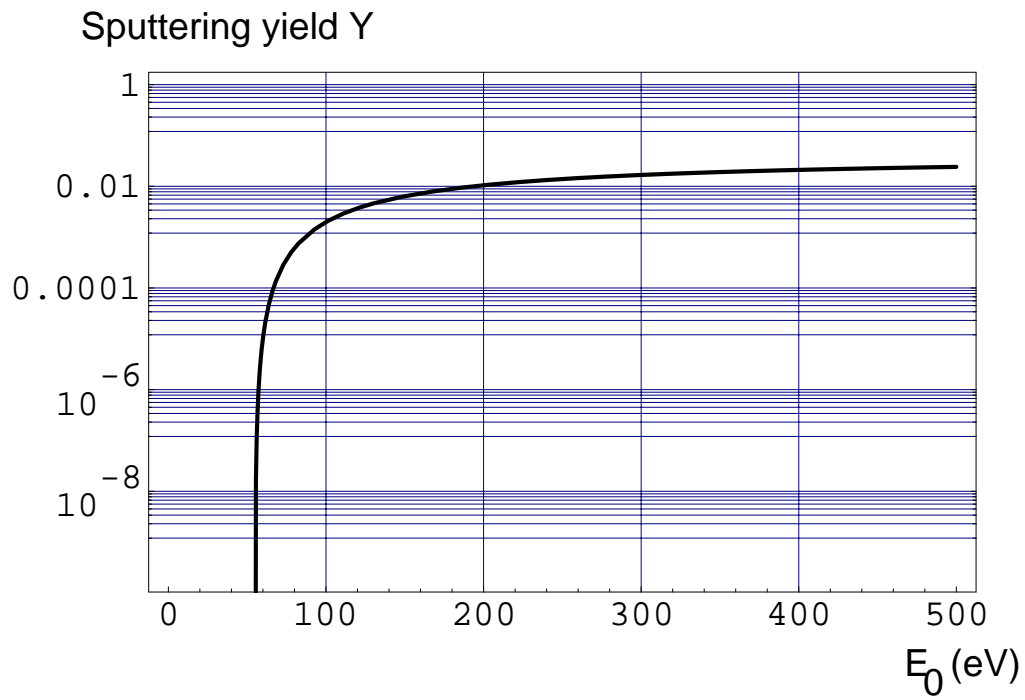Sputtering yield Y

Sputtering yield Y

Figure 22: Sputtering yield versus impact energy (in eV) for protons on copper and copper on copper.

One question that still remains open is the contribution to sputtering from hydrogen atoms (protons) which almost exactly move in the $x-z$ plane under the influence of a resonant dipolar field. As demonstrated above, such protons can in fact be accelerated to multi-keV energies. In addition, the probability is high that these ions hit the beam pipe at a shallow angle because of their circular motion. This will aggravate their effect, since for oblique incidence the sputtering yield is enhanced. This effect may be compounded by the fact that ions produced by beam ionization or synchrotron light ionization will mostly lie in the horizontal plane or close to it. For further studies of the importance of these peculiar ions, more detailed knowledge of angular-dependent sputtering and molecular desorption yields would be required. On the positive side, we note that the resonance condition will be crossed rapidly during ramping of the accelerator.

7 Equilibrium Density

From the information collected throughout this note, we deduce that ions in the beam pipe are produced at a rate 0.012-0.12 s^{-1} and are lost after a typical time of a few μs at most. We have simulated the pattern according to which the ions are lost in time. An example for hydrogen ions in a field-free region of LHC is shown in Fig. 23. The decay of the ions after their generation is well parametrized by

$$\frac{\rho_{\text{ion}}(t)}{\rho_0} = \begin{cases} \left[1 - \left(\frac{t}{\tau_{\text{sur}}}\right)^2\right]^{1/2} & t < \tau_{\text{sur}} \\ 0 & t \geq \tau_{\text{sur}} \end{cases},$$

where we have introduced a maximum survival time τ_{sur}, which can be inferred from simulations for each ion species.

Also defining the ionization time τ_{ion}, we can approximately describe the evolution of the ion density ρ_{ion} by the differential equation

$$\frac{d\rho_{\text{ion}}}{dt} = \frac{\rho_{\text{gas}}}{\tau_{\text{ion}}} - \frac{\rho_{\text{ion}}}{\tau_{\text{sur}}}.$$

Integrating this equation for typical numbers $\tau_{\text{ion}} = 10$ s, $\tau_{\text{sur}} = 1$ μs and $\rho_{\text{gas}} = 10^{15}$ m^{-3} (30 nTorr vacuum pressure), we can numerically determine $\rho_{\text{ion}}(t)$ and its equilibrium value.

Figure 24 shows the time profile of the ion density in the beam pipe. Because of the large difference between ionization and loss rates, a steady state is reached immediately after the time τ_{sur}. The final number of ions thus obtained is not expected to affect the evolution of the electron cloud, because it is 5–6 orders of magnitude lower than the equilibrium electron density.
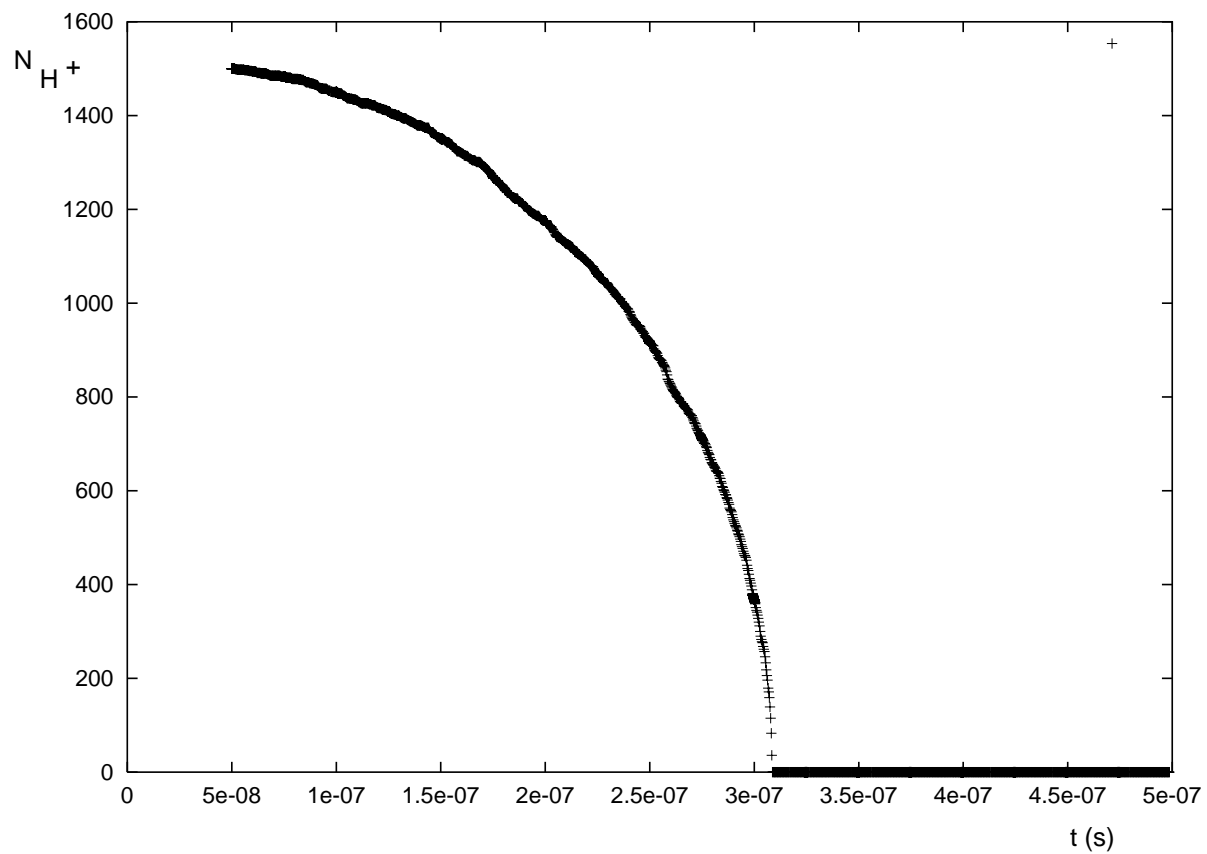
Figure 23: Number of ions in the beam pipe as a function of time. In this simulation we launched 1500 H^+ ions at time $t = 50$ ns.
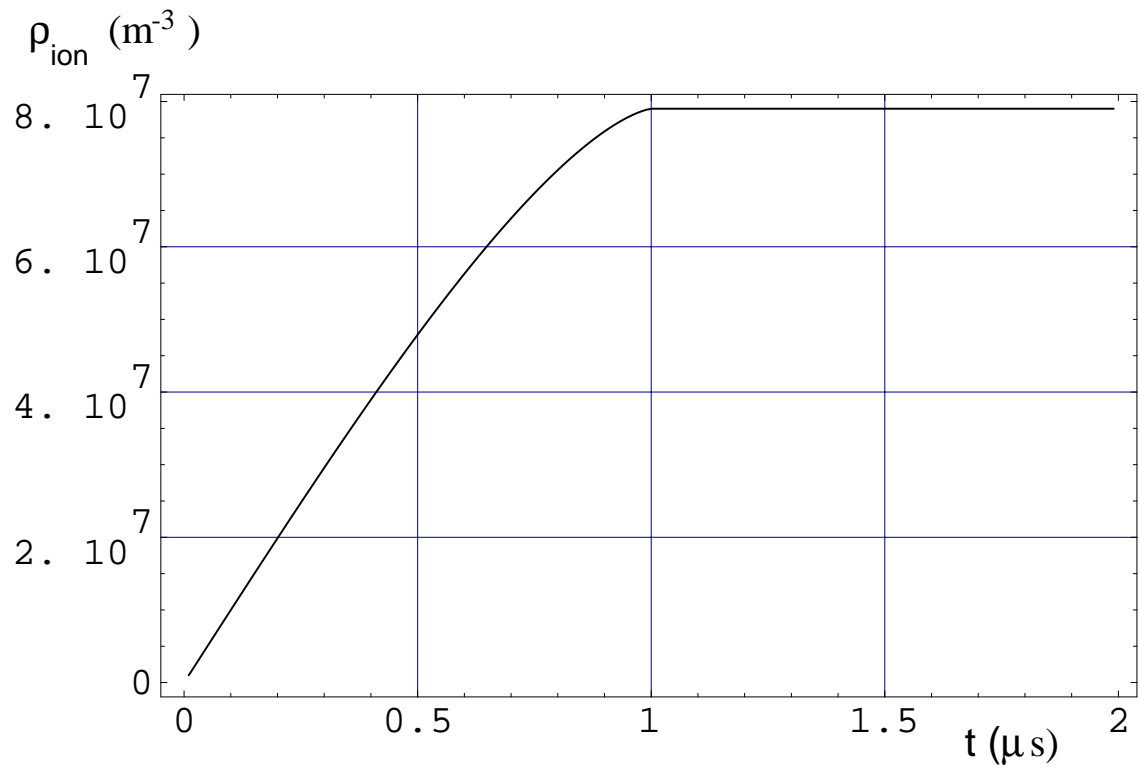
Figure 24: Time evolution of the ion density inside the beam pipe.

8 Conclusions

We have investigated a possible interplay of ions and the electron cloud, using both analytical and simulation approaches.

Although the electron cloud enhances the generation of ions from the residual gas, the survival times of ions generated during the beam passage amount to only a few microseconds and thus do not allow a significant ion accumulation. In particular, estimated equilibrium ion densities are many orders of magnitude smaller than the electron densities and, therefore, the ions will not affect the electrons or the beam.

Ion impact energies usually stay below 200 eV, except for the special case of a dipole field with ion cyclotron period equal to an integer multiple of the bunch spacing, where a small fraction of ions, created with negligible vertical displacement with respect to the beam ($y \approx 0$), can acquire a large horizontal momentum and energies up to several tens of keV.

We have finally assessed the importance of ion reflection and sputtering, and found both effects to be small for the typical ion impact energies inferred from our simulation.

9 Acknowledgements

References

[1] G. Arduini, "Observations in the SPS: Beam Emittance, Instabilities", in *Proceedings of the Workshop on LEP-SPS performance -Chamonix X-, Chamonix, 2000* edited by P. Le Roux, J. Poole and M. Truchet (CERN-SL-2000-007 DI) p. 123-129.

[2] G. Arduini, "Observations on Transverse Instabilities", in *Proceedings of the LHC Workshop -Chamonix XI-, Chamonix, 2001* edited by J. Poole, J. Karlson-Forestier, P. Le Roux, M. Truchet (CERN-SL-2001-003 DI) p. 125-134

[3] K. Ohmi, Phys. Rev. Lett. **75**, 1526 (1995).

[4] M. A. Furman and G. R. Lambertson, in *Proceedings of the International Workshop on Multibunch Instabilities in Future Electron and Positron Accelerators, Tsukuba, KEK 1997* edited by Y. H. Chin (KEK Proceedings 97-17, 1997) p. 170.

[5] F. Zimmermann, "Electron-cloud simulations for SPS and LHC", in *Proceedings of the Workshop on LEP-SPS performance -Chamonix X-, Chamonix, 2000* edited by P. Le Roux, J. Poole and M. Truchet (CERN-SL-2000-007 DI) p. 136.

[6] G. Rumolo, F. Ruggiero and F. Zimmermann, Phys. Rev. ST Accel. Beams, **4**, 012801 (2001).

[7] "Session IV: Electron Cloud Effects, Vacuum (SPS+LHC) in *Proceedings of the LHC Workshop -Chamonix XI-, Chamonix, 2001* edited by J. Poole, J. Karlson-Forestier, P. Le Roux, M. Truchet (CERN-SL-2001-003 DI) p. 136-177

[8] O. Grobner, comment at Chamonix XI.

[9] S.T. Perkins, D.E. Cullen, S.M. Seltzer, "Tables and Graphs of Electron-Interaction Cross Sections from 10 eV to 100 GeV Derived from the LLNL Evaluated Electron Data Library (EEDL), Z=1–100, UCRL-50400-Vol. 31 (1991).

[10] K. Oide, presentation at Chamonix XI.

[11] M. Bassetti and G. Erskine, CERN ISR TH/80-06 (1980).

[12] E. Perevedentsev, "Periodic Solenoid Field", unpublished note, KEK, November 2000.

[13] Nuclear Fusion, Journal of Plasma Physics and Thermonuclear Fusion. **Special Issue 1984** "Data Compendium for Plasma-Surface Interactions" edited by R. A. Langley, J. Bohdansky, W. Eckstein, P. Mioduszewski, J. Roth, E. Taglauer, E. W. Thomas, H. Verbeek,K. L. Wilson (1985).

[14] Nuclear Fusion "Atomic and Plasma-Material Interaction Data for Fusion" (Supplement to the the journal Nuclear Fusion) Vol. 1, edited by R. K. Janev (1991)

[15] H.H. Andersen and H.L. Bay, "Sputtering Yield Measurements," p. 176.